www.czasopisma.pan.pl PAN www.journals.pan.pl
Opto-Electronics Review 27 (2019) 363–368

Contents lists available at ScienceDirect

Opto-Electronics Review

journal homepage: http://www.journals.elsevier.com/opto-electronics review

Design and development of original WSN sensor for suspended particulate matter measurements

L. Makowski[a], B. Dziadak[a,*], M. Suproniuk[b]

[a] Warsaw University of Technology, Institute of Theory of Electrical Engineering, Measurement and Information Systems, 75 Koszykowa St., 00-662, Warsaw, Poland
[b] Military University of Technology, 2 Kaliskiego St., 00-908, Warsaw, Poland

ARTICLE INFO

Article history:
Received 1 July 2019
Accepted 27 November 2019
Available online 25 December 2019

Keywords:
Air quality
Atmospheric measurements
Electronic circuits
Optoelectronic and photonic sensors

ABSTRACT

This paper comprehensively presents key issues in design of an original optoelectronic measurement device built to assess amount of suspended particulate matter. The paper is introduced with a short explanation of concerns with a suspended particulate matter, what role it has in the air quality and how it affects health of human population. Then, problems of construction of the measurement device supported by a theoretical explanation on the basis of Mie theory are discussed. Subsequently, it is followed by an analysis of the device operation both in laboratory and in real conditions. Results obtained with the presented device are compared with the professional measurement equipment and an expensive, outdoor measurement station. Paper is concluded with observations of differences in spatio-temporal PM change at very close but significantly different city locations.

1. Introduction

Air quality is one of key factors that are shaping quality of life in ever-growing cities and conurbations. Global research accomplished on behalf of WHO shows that majority of population (91 %) lives in places where normative limits for air quality are breached [1,2]. Such situation is observed in developed, as well as in developing countries. There is a variety of causes in different places on Earth, but deterioration of standard of living and harmful effects on health of the population are the same.

It is worth to note that according to WHO observations 4.2 millions of people died due to a too high amount of suspended particulate matter (PM) in 2016 alone [3]. PM in the air comes mainly from three significant sources [4]:

- natural sources: erosion of the Earth crust and volcanic eruptions,
- primary: combustion of fossil fuels,
- secondary: formed due to chemical reaction of precursor compounds such as nitrogen oxide, sulfur dioxide, ammonia and volatile organic compounds (VOC).

Particulate matter might be categorized due to particle size as follows:

- Total Suspended Particles (TSP) – includes particles of all diameters, so it includes PM10, PM2.5 and PM1 described below,
- PM10 – consists of inhalable particles with average diameters below 10 μm (so it contains also PM2.5 and PM1); because of their size they might reach upper parts of respiratory tract and lungs;
- PM2.5 - consists of inhalable particles with an average diameter below 2.5 μm; dust particle having this size may penetrate pulmonary alveoli, breach the air-tissue boundary and then invade the cardiovascular system by which it may get to other organs such as the brain;
- PM1 – dust particles with average diameters smaller than 1 μm.

Particulate matter carries toxic molecules and compounds such as cadmium, arsenic, nickel, lead and polycyclic aromatic hydrocarbons (PAHs) such as benzo(a)pyrene. Inhalation of PM significantly increases risk of respiratory diseases such as allergies, asthma, inflammations and pneumonia. Deposits of particles in pulmonary alveoli hinders efficiency of gas exchange. PM2.5 increases not only risk of respiratory tract afflictions but also cardiovascular system diseases such as heart attacks. Due to the fact that by blood circulation particles can reach the brain they are also linked with an increased risk of brain tumors.

Effects on human health discussed above are undoubtedly serious and billions of people living in municipal areas are endangered. Therefore, WHO legislated limits for specific substances that may be observed in the Earth atmosphere and are linked with diseases.

* Corresponding author.
E-mail address: bogdan.dziadak@ee.pw.edu.pl (B. Dziadak).

https://doi.org/10.1016/j.opelre.2019.11.005
1230-3402/

Table 1
Average seasonal values of significant air quality parameters in 2016 [4].

EU/WHO limits(24 hour average)	PM10 [μg/m^3]	PM2.5	NO_2	O_3	Benzo(a)pyren [ng/m^3]
	50	25	40	120	1
Warsaw	66.5	22.5	56.7	111	1.5
Vilnius	51.4	29.4	38.5	89.9	0.9
Stockholm	43.4	6.1	42.8	88.7	–

Some of these values and real data from long-term measurements in three European cities are shown in Table 1. It is worthy to note that some countries, such as Poland, established their own limits of substances and different air quality levels because the situation may be far from desirable there.

Particulate matter naturally deposits on the Earth due to gravity, but other factors such as winds or road traffic might raise it again. Hence, the closer to Earth surface the higher accumulation of PM is observed in the atmosphere. Therefore, higher exposure to risks discussed above is observed in age group of children also because youngsters are more active physically outside home than adolescents and adults. Other endangered groups are those who already have pulmonary and cardiovascular problems and the elderly [5].

2. Monitoring of air quality

Monitoring of air parameters is necessary to evaluate status of the environment, assess quality of life in residential areas and track spatial distribution of pathogenic factors. Measurement methods vary in reference to time range and physical dimensions of the area under observation. The highest accuracy of measurements is obtained with chromatography and gravimetric methods [6,7]. These methods are considered to be a reference methods by many organizations and governmental bodies. However, these two methods have also their significant drawbacks such as: considerable costs of implementation and maintenance, necessity to involve human operators and difficulty in automation.

On the other hand vast areas can be effectively inspected with satellite systems that employ numerical analysis of photographs of the Earth surface taken at many different wavelengths [8,9]. Such constellation of six satellites is cornerstone for Copernicus Atmosphere Monitoring Service established by EU. This system employs seven numerical models and achieves spatial resolution of 100 km^2. However, if reference methods are compared with satellite imaging the differences appear [10]. Satellite imaging is good for long-term observations of large areas, but its limited spatial resolution brings substantial error for city dwellers who are affected by conditions changing not only from district to district but also from street to street.

The most popular approach in a PM sensor design is based on well known and unquestionably cheaper method based on optical sensors. For example PMS 5000/3000 is popular among hobbyists, as well as it is often employed in inexpensive measurement devices that are commercially available to wide range of public customers, and was successfully used in research attempts [11,12]. Such sensors were also deployed in Building Management Systems based on KNX network to monitor interior air quality in homes and offices [13,14]. Despite such low-cost equipment that is popular and provides satisfactory results as if compared against expensive reference methods, it is hard to find exact information about its metrological parameters and precise information about capabilities of devices employing it. Comparative measurements with conditions controlled in laboratory are possible approach to this issue [15]. Whereas in Ref. 16 very high sensitivity optical instruments for NO_x measurement to detect explosives, based on Cavity Ring–Down Spectroscopy with violet laser were presented. Future trend of a low cost sensor, for air quality monitoring was presented [17] where an inkjet printing sensor for CO_2 concentration measurement was described.

Solutions for air quality measurements based on optoelectronics evolved in recent years from simple designs based on a single LED, an uncomplicated mechanical construction and an elementary photodiode. Therefore, it may be deduced that further attempts in this area will bring low-cost devices closer to reference methods.

3. Sensor

Authors of this paper designed a sensor that is presented here. This instrument is based on a nephelometric method that is the measurement of light scattered by particulate matter suspended in the air. This method is known to work well both for liquid and gaseous dispersing mediums [18,19].

Light scattering on aerosol particles can be divided into two groups that are known as inelastic and elastic scattering. Inelastic scattering is characteristic by the fact that scattered ligth has different wavelength that the incident light. In this category we may distinguish phenomena such as fluorescence, thermal emission and Raman scattering. This paper is based on elastic scattering in which reflection and refraction play dominant role. In both of these phenomena the emitted light has the same wavelength as incident light. The particle might be considered as a dielectric obstacle on the path of the light. Particle radius r and the wavelength λ might be compared according to the simple equation:

$$x = \frac{2\pi r}{\lambda}. \tag{1}$$

If x « 1, then the scattering might be described by Rayleigh theory. It happens for very small particles such as gaseous ones. Particulate matter and dust suspended in the air are much larger, therefore x for visible and NIR light is above 1. For such situation solution for Maxwell equations is given by Mie theory that simplifies computational effort and enables quick estimation of scattering characteristics. Simplification is based on assumption that particles are spherical and homogeneous. According to Mie theory intensity of light scattered on single particle [20] might be described as in Eq. (2):

$$I = I_o\left(\frac{\lambda^2}{8\pi d^2}\right)(i_1 - i_2). \tag{2}$$

In the above equation I_0 is the intensity of incident light. The distance between particle on which the scattering occurs and detector equals to d. Scattered light is also polarized and as such it might be described in perpendicular polarization planes given by the functions i_1 and i_2 that can be represented as series shown in Eqs. (3) and (4), respectively:

$$i_1 = \left|\sum_{n=1}^{\infty}\frac{2n+1}{n(n+1)}[a_n\pi_n(\cos\theta) + b_n\tau_n(\cos\theta)]\right|^2. \tag{3}$$

$$i_2 = \left|\sum_{n=1}^{\infty}\frac{2n+1}{n(n+1)}[a_n\tau_n(\cos\theta) + b_n\pi_n(\cos\theta)]\right|^2. \tag{4}$$

Here θ is the scattering angle while the angular dependent functions π_n and τ_n are expressed in terms of the Legendre polynomials given with equations:

$$\pi_n(\cos\theta) = \frac{P_n^{(1)}(\cos\theta)}{\sin\theta}. \tag{5}$$

$$\tau_n(\cos\theta) = \frac{dP_n^{(1)}(\cos\theta)}{d\theta}. \tag{6}$$

Terms a_n and b_n are known as the Mie expansion coefficients that can be expressed as follows:

$$a_n = \frac{\Psi_n(\alpha)\Psi_n'(m\alpha) - m\Psi_n(m\alpha)\Psi_n'(\alpha)}{\xi(\alpha)\Psi_n'(m\alpha) - m\Psi_n(m\alpha)\xi_n'(\alpha)}. \tag{7}$$

$$b_n = \frac{m\Psi_n(c)\Psi_n'(m\alpha) - \Psi_n(m\alpha)\Psi_n'(\alpha)}{m\xi_n(\alpha)\Psi_n'(m\alpha) - \Psi_n(m\alpha)\xi_n'(\alpha)}. \tag{8}$$

where:

m - complex reflective index of scattering light intensity;

α - size parameters;

Ψ and ξ- coefficients expressed in terms of the Riccatti-Bessel functions of non-integer order.

Therefore, an expression might be defined relating to the particulate matter concentration C with the scattered light intensities i_1 and i_2 (9):

$$C = \frac{4\pi^3 r^2 \rho(\frac{I}{I_0})}{3\lambda^2 kS\sum_i \frac{i_1+i_2 nd(D_n)}{D_i^3}\Delta D}. \tag{9}$$

where ρ is the density of suspended particles, D is the diameter of particle, and $nd(D_n)$ is the mass size distribution normalized function of dust particles, n relates to the number size distribution of the particles and k is the direction of gas flow, and S is the cross-sectional of the air track.

From the above equation it might be concluded that to obtain a representative sample of the analyzed air is crucial for a proper measurement of a suspended particulate level and, then estimate atmosphere quality. Crucial for the measurement of atmosphere quality is to obtain a representative sample of the analysed air. Therefore, the key component of the sensor is an air intake and air track that is described in the next section.

3.1. Air track

Automation of the measurement system based on the optoelectronic method is possible in long-term provided that cohesion of a gaseous sample is guaranteed. By cohesion of the sample we understand that it is a representative sample of the air currently present outside of the sensor. This can be achieved with a constant air flow but minimal turbulence inside the track. Unfortunately, the higher the flow the more turbulent it becomes. Hence, the main consideration to achieve this goal is to secure laminar flow of the air in the air track or at least in the zone near photodetector. We looked for the maximum possible air flow value without risking turbulent behaviour.

Laminarity of the flow is defined by Reynolds number (Re) and there is a specific value of Re for every evaluated air track. Flow is considered to be laminar when the Reynolds number Re is below 2300 [21]. In the following calculations temperature of the air was assumed to be of 20°. Air flow can be calculated with the following Eq. (10):

$$v = \frac{Re \cdot vi}{l}, \tag{10}$$

where, for presented sensor:

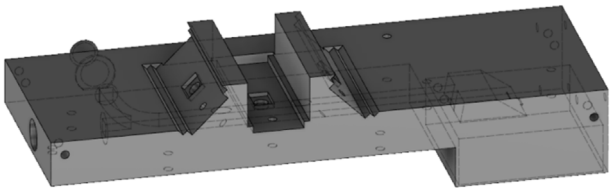

Fig. 1. Model of a 3D-printed support for mainboard, opto-electronic modules, laser and fan, inside of which the air track is present.

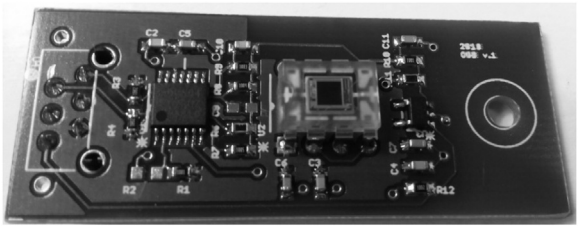

Fig. 2. Opto-electronic module with an integrated photodiode and an amplifier with supporting multiplexer in the feedback loop.

- kinematic viscosity $vi = 0.0000157$ m^2/s;
- characteristic dimension l =0.005 m;
- maximum value of Reynolds number Re = 2300.

After this simple computation a boundary for speed of laminar air flow is found: v =7.22 m/s. Therefore, absolute volumetric flow in the designed track geometry equals: V_{max} = 0.000180 m^3/s = 10.8 l/min.

As it is upper boundary the real speed of the air flow in the built sensor was lowered. In order to guarantee a stable and laminar flow value, the air track is coupled with the flow control system based on a fan propelled with BLDC engine. Adjustment of the air flow speed is voltage-regulated in the range from 0.3 to 1.0 l/min. Sketch view of the air track with slots for optoelectronic detectors and laser is shown in Fig. 1.

3.2. Optoelectronic detector

Optoelectronic detector module is presented in Fig. 2. It is based on Texas Instruments' chip (OPT101) that is a photodiode integrated with a transimpedance operational amplifier. Thanks to this integration distortions and noise are minimized which always happens on the path between photodiode and the opamp. The built-in amplifier has an internal resistor for negative feedback, but an external element may be also used instead. In the presented design a feedback loop is chosen from four possible options with the use of an analog multiplexer managed from the microcontroller on the device mainboard. Availability of four different feedback resistors makes it possible to use whole range of sensitivity provided by the chip. Therefore, it is possible to employ presented module in different air quality conditions: starting from typical air quality present in houses or offices up to dusty industrial buildings.

3.3. Mainboard of the measurement device

Mainboard is a hub for optoelectronic sensors presented in the previous section. Three of such sensors might be connected to a single board for improved versatility. Because the connection is wired, then one sensor might be placed inside while the other outside and the third one behind a filter that purifies the air towards zero-air quality. In the current development stage all three sensors are placed close one to another by the same air track presented above.

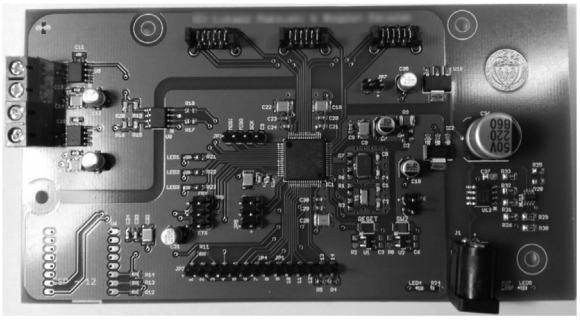

Fig. 3. Mainboard for the measurement device with STM32 microcontroller, voltage regulators, laser control circuitry, hub for photodiode modules and additional pinout connectors for future use.

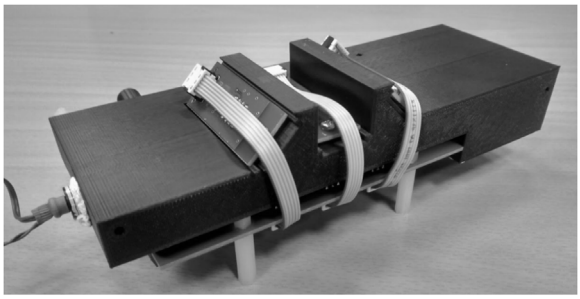

Fig. 4. Real view of a 3D-printed support block assembled together with all electronic modules and components.

In this configuration we measure a backward, perpendicular and forward scatter.

Photo of the mainboard is presented in Fig. 3. Its physical dimensions are of 70 mm by 130 mm. The board is based on the mixed signal microcontroller STM32 with ARM Cortex-M4 core. The chip is capable of floating-point calculations which is a very useful feature for development of computational functions in the described system. This MCU has lavish 512 kB of flash memory for program code and 80 kB of SRAM which is enough at the current stage of development. Internal clock tops with 72 MHz and is driven by external crystal oscillator for improved signal quality and system stability. Existing functionality of the software does not require higher parameters and the chosen MCU is cheap enough to remain insignificant in the overall cost of the board.

Analog signal from optoelectronic modules is converted with analog-digital converters providing typical, 12-bit resolution, that is 4096 possible values.

Another task that mainboard does is control of the laser light source. Voltage applied to a laser module is controlled thanks to a typical circuit of MOSFET transistors connected to GPIO of the MCU and handled by software deployed there.

Laser module is a typical 660 nm visible red light laser that illuminates the measured air sample. In early experiments we verified that it is possible to modulate the used laser up to several kHz frequency. However, during later examination we found that in practice a much better result is obtained with a continuous wave. Laser is turned on and off periodically with a long time interval. Outcomes of this approach are as follows:

- it becomes possible to measure photodiode dark current which is essential contribution to noise level,
- energy is conserved, which is an important feature, if a device is to be powered from battery or solar panel,
- risk of heating of the laser or other device parts that are illuminated by its light is prevented.

In its current form mainboard is supposed to be supplied through a typical 5.5 mm/2.1 mm Jack connector, so that it is possible to use a typical switched-mode power supply. The board contains a segment of voltage regulators with overvoltage and undervoltage protection. Possible range of applied voltage is simply chosen by values of three resistors so during the manufacturing process it might be easily modified for specific needs of customer or application.

3.4. Software features

Software template was prepared with STM32CubeMX application that simplifies configuration of the MCU and reduces time to launch development of the application. Configured MCU features include USART communication channel through which the measurements are presented, analog-digital converters, several GPIO ports to control laser and on-bard LED diodes. Program was written in System Workbench for STM32 environment that is based upon well known and popular Eclipse IDE with use of C language.

ADC is driven by main clock signal 72 MHz that is divided by the prescaler value. We experimented with different ADC clock speeds and different times of sampling to finally conclude that frequency of several kHz is the optimal choice due to quality of observed signal details and requirements for memory and computational efficiency of the MCU.

Air track joined with electro-optical modules, mainboard and laser is presented in Fig. 4. This assembly was enhanced with mounting power supply and secured in enclosure. Then, it was put under tests both inside and outside the building.

4. Results

The device was put under the series of tests consisting of two stages. First stage was to verify the optoelectronic module behavior in controlled, laboratory conditions. Second stage was to analyze operation of the whole device both in laboratory and real conditions.

For the purpose of the first stage a laboratory stand was established to test the sensor in a wide range of PM amount in the air. To procure air sample with dust we used $(K,Na)_{2\text{-}3}(OH,F)_2(Si,Al_4O_{10})$ mica powder with particle diameters up to 20 μm. Thanks to this approach we were able to create brief dust concentrations up to 10 mg/m^3. This level of PM is observed in industrial situations, e.g., drilling of concrete walls or sawing of sidewalk blocks and certainly requires personal protection such as respiratory mask. During this experiment we used commercially available Trotec PC220 as a reference device measurement for comparative method. Voltage signal from the photodiode was acquired with high quality Teledyne LeCroy WaveSurfer 3000 oscilloscope. Signal acquisition in single attempt lasted for 30 min.

It is known that spatial characteristics of scattered light depends on observation angle, particles' size and irradiating light wavelength. But in general the smaller the particle is, the smaller will be the observed signal at a given angle. In our configuration the signal from backscatter and forward scatter detectors was more significant with higher levels of concentration which adheres to scattering theory. Interesting part of the acquired signal is shown in Fig. 5.

Second stage of tests engaged experiments with low PM concentrations at levels that are more typical for urban areas, houses and offices. At this phase the whole device was put under investigation. Temperature in the laboratory room was equal to 21 ◦ and the airflow was set to 0.32 m/s. Typical particle that was moving at this speed remained in the measurement chamber for time shorter than 20 ms. Acquisition of the signal presented in Fig. 6 lasted 120 min.

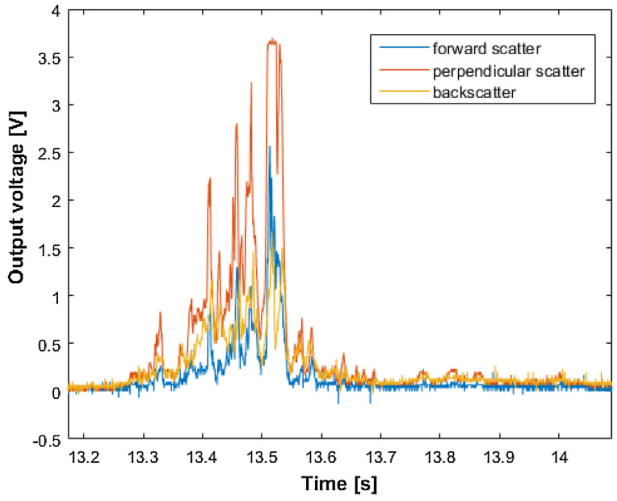

Fig. 5. Short-term analysis of raw signal from the opto-electronic module.

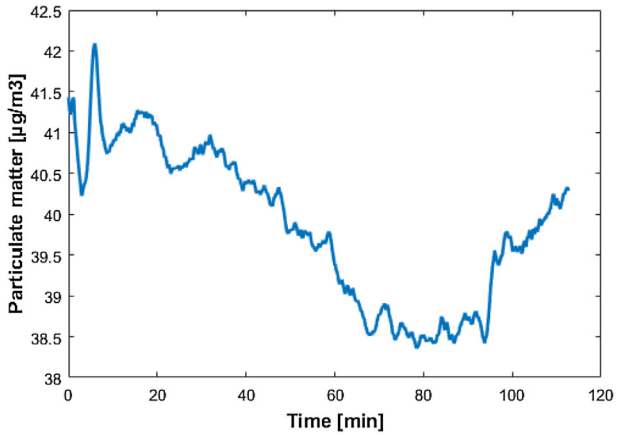

Fig. 6. Mid-term signal from the device working in room conditions.

At the beginning there were people present in the room and moving so that particles could not have settled. Later the room was left empty and closed so that PM deposition took effect and less particles entered the measurement chamber. It can be observed in the figure as a slowly decreasing signal between 40 and 90 min. Then, one person returned to the room which reversed the deposition of PM. This experiment shows that a larger PM presence in the air creates a long-term issue as the previously deposited dust may become a problem again. Similar situation is observed on city streets where traffic creates turbulences in the air that are effectively raising dust from road lanes and re-introduce it into the air.

Then, we analyzed quantitative distribution of distinctive dust fractions derived from particle sizes on the basis of the exemplary measurement period, which is presented in the above plot. Result of this analysis is presented on a histogram shown in Fig. 7. In the optical sensor low response signal level corresponds to detection of small particles while high signal appears when particles have higher diameters. Therefore, we can observe that there is more dust particles with smaller diameters and that the amount of particles per group drops abruptly as their diameter increases. This relation is widely known and universal among locations. It was confirmed by experiments in Greece and China [22], and having it here affirms proper functioning of the sensor.

Finally, the measurement device was set up outside and put under long-term test under real conditions. As a reference we used a professional measurement station maintained by governmental

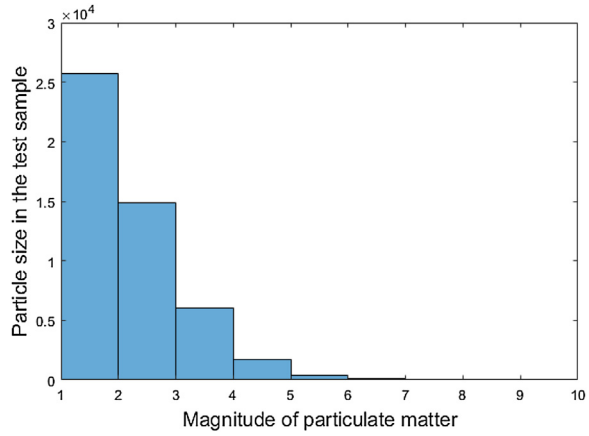

Fig. 7. Distribution of particle size in the test sample.

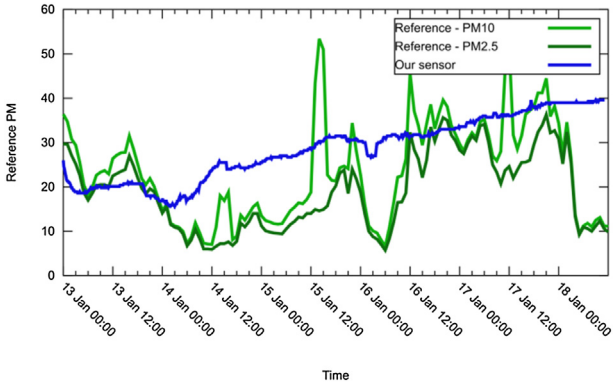

Fig. 8. Long-term signal acquisition from the device presented in this paper compared with the nearby reference station maintained by government agency.

body which provides publicly available data. Distance between our station and the reference station measured on straight line is just 300 m. However, there are crucial differences between both places and they must be taken into account during comparison. Reference station is placed just by six lane road to measure PM caused by road traffic. Between this place and our station there are several buildings and our station is far from any significant traffic. Shortest distance between our station and road equals 70 m. Therefore, it may be expected that our station will be less affected by weekday morning and afternoon traffic increase during rush hours. On the other hand wind should have lesser effect on our station than on the reference station as our position is shadowed by buildings and is a significantly less windy location. This long term comparison with both effects visible is presented in Fig. 8.

5. Conclusions

In the paper we presented the comprehensive approach to design of hardware and software of a particulate matter sensor. Device is based mostly on surface-mounted components where the key part is STM32 microcontroller controlling a laser module and photodiode boards, performing initial signal processing and transmitting resulting data. Laser light source and three photodiodes at different angles coupled with an efficient microcontroller enable both high sensitivity and high temporal resolution of measurements.

3D printing was used to stimulate rapid development of air tract so that optimal structure with minimized Reynolds number (Re) in the range from 130 to 300 was accomplished. This guarantees laminar flow, hence there are less disturbances in the particulate matter

distribution in the analyzed air and reliability of measurements is improved.

Verification both in laboratory and in real conditions of our new measurement device characteristics was discussed. Experiments include short-term test of the optoelectronic module in the laboratory-controlled environment, medium-term verification in office room conditions and long-term study outdoors where the device was exposed to various weather conditions during three winter months. Laboratory test lead to a conclusion that the sensor works correctly. Firstly, its output signal follows change with low levels of particulate matter. Secondly the distribution of particulate sizes in the sample is as it should be expected theoretically. In the field conditions measurements were compared with results from the reference station that is positioned at a distance of 300 m in straight line from our experiment site. Despite the fact that distance was considerably large the trend of results from the sensor presented in the paper follows the trend acquired from governmental station. Analysis of measurement error will be the main subject in next stage of our research.

Finally, it may be concluded that the opto-electronic measurement device is a low-cost design that certainly cannot challenge the excellence or resolution of reference methods, but it can successfully join and have positive impact on existing networks that were established for measurements of air quality.

Acknowledgements

This work was partially funded by grant POIR.04.04.00-00-0004/15, MNISW/2017/DIR/75/II+in cooperation with IBS sp. z o.o.

References

[1] J.O. Anderson, J.G. Thundiyil, A. Stolbach, Clearing the air: a review of the effects of particulate matter air pollution on human health, J. Med. Toxicol. 8 (2012) 166–175, http://dx.doi.org/10.1007/s13181-011-0203-1.
[2] World Health Organization (Ed.), Who Guidelines for Indoor Air Quality: Selected Pollutants, WHO, Copenhagen, 2010.
[3] Ambient (outdoor) air quality and health, 2016.https://www.who.int/news-room/fact-sheets/detail/ambient-(outdoor)-air-quality-and-health (Accessed 28 June 2019).
[4] Explore air pollution data, European Environment Agency. 2016. https://www.eea.europa.eu/themes/air/explore-air-pollution-data (Accessed 28 June 2019).
[5] D. Brook Robert, Rajagopalan Sanjay, Pope C. Arden, R. Brook Jeffrey, Bhatnagar Aruni, V. Diez-Roux Ana, Holguin Fernando, Hong Yuling, V. Luepker Russell, A. Mittleman Murray, Peters Annette, Siscovick David, C. Smith Sidney, Whitsel Laurie, D. Kaufman Joel, Particulate matter air pollution and cardiovascular disease, Circulation 121 (2010) 2331–2378, http://dx.doi.org/10.1161/CIR.0b013e3181dbece1.
[6] B.L.V. Drooge, D.R. García, S. Lacorte, Analysis of organophosphorus flame retardants in submicron atmospheric particulate matter (PM1), Environmental 5 (2018) 294–7304, http://dx.doi.org/10.3934/environsci.2018.4.294.
[7] M. Kraus, I.J. Šenitková, Particulate matter mass concentration in residential prefabricated buildings related to temperature and moisture, IOP Conf. Ser.: Mater. Sci. Eng. 245 (2017) 042068, http://dx.doi.org/10.1088/1757-899X/245/4/042068.
[8] Y. Zhang, Z. Li, Remote sensing of atmospheric fine particulate matter (PM2.5) mass concentration near the ground from satellite observation, Remote Sens. Environ. 160 (2015) 252–262, http://dx.doi.org/10.1016/j.rse.2015.02.005.
[9] M. Sowden, U. Mueller, D. Blake, Review of surface particulate monitoring of dust events using geostationary satellite remote sensing, Atmos. Environ. 183 (2018) 154–164, http://dx.doi.org/10.1016/j.atmosenv.2018.04.020.
[10] A. Hys, J. Dumańska, K. Tworek, Stężenie pyłów zawieszonych PM10 w Polsce w 2015 roku – porównanie danych z serwisu CAMS programu Copernicus z danymi Głównego Inspektoratu Ochrony Środowiska, Metrologia i Probiernictwo – Biuletyn Głównego Urzędu Miar. (2018) 12–19 (In Polish).
[11] T. Sayahi, A. Butterfield, K.E. Kelly, Long-term field evaluation of the Plantower PMS low-cost particulate matter sensors, Environ. Pollut. 245 (2019) 932–940, http://dx.doi.org/10.1016/j.envpol.2018.11.065.
[12] K.E. Kelly, J. Whitaker, A. Petty, C. Widmer, A. Dybwad, D. Sleeth, R. Martin, A. Butterfield, Ambient and laboratory evaluation of a low-cost particulate matter sensor, Environ. Pollut. 221 (2017) 491–500, http://dx.doi.org/10.1016/j.envpol.2016.12.039.
[13] K. Gecova, D. Vala, Z. Slanina, W. Walendziuk, in: R.S. Romaniuk, M. Linczuk (Eds.), Air Condition Sensor on KNX Network, Wilga, Poland, 2017, p. 104455U, http://dx.doi.org/10.1117/12.2280810.
[14] A. Stachno, M. Suproniuk, Environmental performance measurement system designed for forecasting in intelligent buildings, Przeglad Elektrotechniczny 89 (2013) 152–155.
[15] D. Liu, Q. Zhang, J. Jiang, D.-R. Chen, Performance calibration of low-cost and portable particular matter (PM) sensors, J. Aerosol Sci. 112 (2017) 1–10, http://dx.doi.org/10.1016/j.jaerosci.2017.05.011.
[16] J. Wojtas, T. Stacewicz, Z. Bielecki, B. Rutecka, R. Medrzycki, J. Mikolajczyk, Towards optoelectronic detection of explosives, Opto-Electron. Rev. 21 (2013) 210–219, http://dx.doi.org/10.2478/s11772-013-0082-x.
[17] B. Andò, S. Baglio, G. Di Pasquale, A. Pollicino, S. Graziani, C. Gugliuzzo, C. Lombardo, V. Marletta, Direct printing of a multi-layer sensor on pet substrate for CO2 detection, Energies 12 (2019) 557, http://dx.doi.org/10.3390/en12030557.
[18] L. Makowski, Low-cost laboratory stand for turbidity measurements, Elektron. Elektrotech. 22 (1) (2016) 49–52, http://dx.doi.org/10.5755/j01.eie.22.1.14108.
[19] H. Hojaiji, H. Kalantarian, A.A.T. Bui, C.E. King, M. Sarrafzadeh, Temperature and humidity calibration of a low-cost wireless dust sensor for real-time monitoring, 2017 IEEE Sensors Applications Symposium (SAS) (2017) 1–6, http://dx.doi.org/10.1109/SAS.2017.7894056.
[20] A. Bain, A. Rafferty, T.C. Preston, Determining the size and refractive index of single aerosol particles using angular light scattering and Mie resonances, J. Quant. Spectrosc. Radiat. Transf. 221 (2018) 61–70, http://dx.doi.org/10.1016/j.jqsrt.2018.09.026.
[21] ISO 5167-1:2003(en), Measurement of fluid flow by means of pressure differential devices inserted in circular cross-section conduits running full — Part 1: General principles and requirements, 2003. https://www.iso.org/obp/ui/#iso:std:iso:5167:-1:ed-2:v1:en (Accessed 28 June 2019).
[22] R. Giere, X. Querol, Solid particulate matter in the atmosphere, Elements 6 (2010) 215–222, http://dx.doi.org/10.2113/gselements.6.4.215.